Thermal characterisation of nanocrystalline porous CePO4 ceramics

Sajan Daniel George, Rajesh Komban, K. G. K. Warrier, P Radhakrishnan, V. P. N. Nampoori, C. P.G. Vallabhan

Thermal characterisation of nanocrystalline porous CePO4 ceramics

Journal:	*Philosophical Magazine & Philosophical Magazine Letters*
Manuscript ID:	TPHM-09-Feb-0086.R1
Journal Selection:	Philosophical Magazine
Date Submitted by the Author:	27-Jun-2009
Complete List of Authors:	George, Sajan; TU Darmstadt, Center of Smart Interfaces Komban, Rajesh; Regional Research Laboratory, Ceramic Technology Division Warrier, K. G. K.; Regional Research Laboratory, Ceramic Technology Division Radhakrishnan, P; Cochin University of Science and Technology, International School of Photonics Nampoori, V. P. N.; Cochin University of Science and Technology, International School of Photonics Vallabhan, C. P.G.; Cochin University of Science and Technology, International School of Photonics
Keywords:	ceramics, nanostructured ceramics, phonons, thermal transport
Keywords (user supplied):	ceramics, nanostructured ceramics, phonons

Thermal characterisation of nanocrystalline porous $CePO_4$ ceramics

Sajan D George[1,3*], Rajesh Komban[2], K. G. K. Warrier[2], P. Radhakrishnan[3], V. P. N. Nampoori[3] and C. P. G. Vallabhan[3]

[1]Center of Smart Interfaces, TU Darmstadt, Petersenstrasse 32, 64287, Darmstadt, Germany

[2]Ceramic Technology Division, Regional Research Laboratory, CSIR, Thiruvanathapuram 695019, India

[3] International School of Photonics, Cochin University of Science and Technology, Cochin 682022, India

[*]Email: george@csi.tu-darmstadt.de

Abstract

In this work, laser induced photoacoustic technique has been employed to investigate thermal transport through nanocrystalline $CePO_4$ samples prepared via sol-gel route. Evaluation of thermal diffusivity is carried out using one-dimensional model of Rosencwaig and Gersho in the reflection configuration of photoacoustic method. Structural analyses of samples show that they are nano porous in nature, possessing micron sized grains. Analysis of results shows that thermal diffusivity value varies with sintering temperature. Results are explained in terms of the variation in porosity with sintering temperature and the effects of various scattering mechanisms on the propagation of phonons through the nanoporous ceramic matrix. Further analyses confirm that apart from porosity, grain boundary resistance and interface thermal resistance influence the effective value of thermal diffusivity of samples under investigation.

Keywords: Photoacoustic, nanocrystalline ceramics, sol-gel method, thermal diffusivity

Introduction

Research towards a better understanding of the physical properties of heterogeneous solids has both scientific and technological importance [1- 2]. In recent years, rare earth phosphates are becoming increasingly important for several applications which include ceramic materials, catalysts, photoluminescence materials, dielectric substrates, metal surface treatment agents, optical materials, etc [3-6]. Other potential applications of these materials include host matrices for immobilization of actinide radio nuclear wastes, solid protonic conductors and weak fiber matrix interfaces in ceramic-ceramic composites or thermal protection coatings [7-10]. Of late, synthesis of nanocrystalline rare earth phosphates has been attempted via various methods such as sol-gel method, surfactant directed hydrothermal approach, etc [11-12]. Cerium phosphate is an important class of rare earth phosphate ceramic, which has immense use in high temperature applications due to its high melting point. Apart from its potential as storage material for nuclear waste and poison to automobile catalyst, recently, it has been used as proton conduction membrane in hydrogen fuel cells [13]. However, the chemical and physical properties of these ceramics depend greatly on the processing technique and conditions. Although various aspects of nanocrystalline ceramics are already investigated, measurement of thermal parameters of sol-gel prepared nanocrystalline $CePO_4$ is not investigated in detail.

Since the proposal of R-G theory of photoacoustic effect in solids [14], photothermal methods have been used for determining several material properties in different states of matter where conventional spectroscopic methods fail [15-17]. Amongst various photothermal techniques, photoacoustic method (PA) has become more popular due to it simplistic approach. The PA effect directly looks into the heat generated in the sample due to non-radiative de-excitation processes following an optical excitation of the sample with modulated

or pulsed light [17]. Data on the thermal properties are vital for any material employed in devices with thermal dissipation. Thermal diffusivity is a unique and important thermophysical parameter, which measures the rate of diffusion of heat in a material. Physically, the inverse of thermal diffusivity is a measure of the time required to establish thermal equilibrium in a system in which transient temperature change has occurred [18-21]. As a result, thermal diffusivity is directly related to micro structure and thereby the processing conditions of ceramics.

In our previous work, we reported thermal characterization of porous $LaPO_4$ ceramics using photothermal technique [21]. In this paper, work is focused on the evaluation of thermal diffusivity of nanocrystalline $CePO_4$ prepared via sol-gel process and the influence of sintering temperature on thermal diffusivity. Sintering is the process whereby interparticle pores in a granular material are eliminated by atomic diffusion driven by capillary forces. The process of sintering can profoundly influence the porosity of nanocrystalline ceramics and thereby the heat transport through materials. Porous ceramics are receiving considerable attention due to its applications in variety of areas such as thermal and noise isolation, liquid and gas infiltration, catalyst products, electronics and biomedical applications [22-24]. Hence, a detailed investigation of the influence of sintering on porosity and hence on thermal diffusivity is of great relevance, especially from the device fabrication point of view.

Sample Preparation

Cerium nitrate, 99.9% pure (M/s Indian Rare Earths Ltd., India) and orthophosphoric acid (AR grade, 88%, Qualigens Fine Chemicals, India) are used as starting materials. A 0.03 M (9.239 g) solution of $Ce(NO_3)_3.6H_2O$ is prepared in de-ionized water. Orthophoshporic acid solution (2,084g, 1.191 mL) is added drop-wise to the cerium nitrate solution under constant stirring. An off-white precipitate of cerium phosphate was obtained. The precipitate is filtered and washed free of nitrates and phosphates, and is further re-dispersed in de-ionized water.

Electrostatic stabilization is achieved by the addition of 20% nitric acid, with the pH maintained in the range of 1.8 – 2. The suspension is stirred continuously for about 4 hours. The colloidal sol thus obtained is further subjected to ultrasonication for 15 minutes to obtain stable cerium phosphate precursor sol. Gelation of the sol is carried out by exposing to ammonia atmosphere for a period of two days. Cerium phosphate gel thus obtained is dried at 80^0C and calcined at 400^0C at the rate 10 ^{0}C/min under air atmosphere to yield Cerium Phosphate gel powder. The relative density of cerium phosphate sintered at different temperatures has been measured using Archimedes displacement method. The porosity p of specimens having relative density x is evaluated knowing that $p = 1 - x$ [25], and is reported in Table I.

The phase identification is carried out by XRD (Philips PW 1710) on the calcined powders using Cu Kα radiation (Figure 1). The gel calcined at 400^0C shows the transformation of rhabdophane to hexagonal form. The major hexagonal cerium phoshpate is identified with JCPDS file no 4-362 and the presence of rhabdophane (JCPDS file no 35-0614) in the XRD pattern also shows the incomplete transformation of hexagonal phase. **Sample calcined at 800^0C shows broad peaks of monazite type monoclinic cerium phosphate (JCPDS file no 32-0199) which became sharp above this temperature**. The crystallite size calculated using X ray line broadening method using Scherrer equation $t = \frac{0.9\lambda}{\beta \cos\theta}$, where t is crystalline size, λ is wavelength of radiation (1.54 Å for Cu Kα radiation), β is the corrected peak width at half maximum intensity, and θ is the angle of diffraction at the peak position, is shown in Figure 2. The crystallite size ranges from 10 to 40 nm and it increases with sintering temperature. The calcined powder was compacted at a pressure of 200 MPa to pellets of size 11 mm and thickness around 500 µm and sintered in the range of 800 to 1700^0C, at a heating rate of 10^0C/min and soaked for 3hours. **BET surface area and pore size distribution of the gel after calcination at 400 and 800 °C were**

measured by nitrogen adsorption after degassing the powders at 200 °C for 4h using Micromeritics Gemini 2375 V5.01 surface area analyzer. The pore size distribution was obtained by Barrett-Joiner-Halenda (BJH) method from the desorption curve of the isotherm using the Micromeritics StarDriver version 2.03 software.

Experimental

A schematic view of experimental set up is shown in Figure 3. Optical radiation from an Argon ion laser at 488 nm (Liconix 5300) is used as the source of excitation, and it is intensity modulated using a mechanical chopper (Stanford Research Systems SR 540) before it strikes the sample surface. Detection of pressure fluctuations (photoacoustic signal) in the cell cavity is done using a sensitive microphone (Knowles BT 1754). The amplitude of the photoacoustic signal is measured using a dual phase lock-in amplifier (Stanford Research Systems SR 830). The laser power used for the present studies is 50 mW with a stability of ± 0.5**%. A homemade PA cell is employed for the present studies. The present cell is made using an acrylic polymer (Perspex) and the volume of the cell is designed such that PA amplitude is maximum but still large enough to avoid thermoviscous damping of acoustic signals at the cell wall. The PA cell is fabricated on the cell material with 5cm diameter and 1cm thickness by drilling bore of diameter 3mm, along its thickness direction, through its center. Another fine bore of diameter 1.5 mm pierced at the middle of the main chamber and directed perpendicular to it serves as the acoustic coupler between the main chamber and the microphone. At a distance of 8mm from the main chamber the microphone is fixed to the orifice of side tube. In this case, the thermal diffusion length in air is smaller than acoustic cell diameter and thus one dimensional model of R-G theory can be used**. More details about the set up can be found elsewhere [26].

Theoretical background

According to one dimensional model of Rosencwaig and Gersho [14], the pressure variation δP at the front surface of an optically thick ($l \gg 1/\mu$, where μ is the optical absorption length) sample irradiated with a chopped beam of monochromatic radiation depends on the thermal diffusivity α_s of the sample. The theoretical expression for δP may be written as

$$\delta P = X.Y \tag{1}$$

In the above expression

$$X = \left[1 + g\frac{h^+ + h^-}{h^+ - h^-}\right]\left[g + \frac{h^+ + h^-}{h^+ - h^-}\right]\frac{1}{\alpha_s^2 l_s^2} \tag{2}$$

Where

$$h^+ = \exp(\sigma_s l_s)$$

$$h^- = \exp(-\sigma_s l_s)$$

and $$\sigma_s = (1+j)\left(\frac{\pi f}{\alpha_s}\right)^{1/2} \tag{3}$$

where $$j = \sqrt{-1} \tag{4}$$

$$g = \frac{e_b}{e_s} = \left(\frac{K_b}{K_s}\right)\left(\frac{\alpha_s}{\alpha_b}\right)^{1/2} \tag{5}$$

is the ratio between effusivities of backing material (e_b) and the sample (e_s) and

and $$Y = \frac{P_o \gamma W_o l_s^2}{2 l_g T_o K_s}\left(\frac{\alpha_s}{\alpha_b}\right)^{1/2} \tag{6}$$

Here l and K indicates the length and thermal conductivity of the corresponding part of the geometry shown in Figure 4 where the subscripts g, s and b refers to gas, sample and backing respectively. $P_o (T_o)$ is the ambient pressure (temperature), γ is the specific heat ratio of air. W_a is the absorbed power of optical radiation. The effusivity of the gas can be neglected in comparison to the effusivity of sample, since their ratio is always less than 1%. The term X depends on the modulation frequency through the product $\sigma_s l_s$, which can be written as

$$\sigma_s l_s = (1+j)\left(\frac{\pi f}{f_c}\right)^{1/2} \quad (7)$$

where characteristic frequency f_c is given by

$$f_c = \frac{\alpha_s}{\pi l_s^2} \quad (8)$$

When thermal diffusion length $\left[d = \left(\frac{\alpha}{\pi f}\right)^{1/2}\right]$ is greater than sample thickness, thermal properties of the backing material determine the PA signal. But in the thermally thick regime, PA signal is independent of the thermal properties of backing material. For a given sample thickness, there is a transition from thermally thin regime to thermally thick regime with variation in chopping frequency. Such a transition is exhibited in the amplitude spectrum of PA signal, which is evinced by the change in slope and by knowing the transition frequency and thickness of the specimen; thermal diffusivity can be evaluated using equation (8).

Results and Discussions

Initially, the experimental setup used for the investigation is calibrated by evaluating the thermal diffusivity of GaAs and Al. The measured values of thermal diffusivity (0.260 ± 0.03 cm^2s^{-1} and 0.978 ± 0.03 cm^2s^{-1} respectively) agree well with earlier reported values [18, 27]. Figure 5 shows the amplitude spectrum of PA signal for sample sintered at 800^0C. All other samples show similar behavior (not shown here). The thermal diffusivity values of cerium phosphate sintered at different temperatures was evaluated from the amplitude spectrum of PA signal and is given in Table I. From the values, it is obvious that sintering temperature affects porosity of the specimen and thereby influences the thermal diffusivity value. Thermal transport properties of polycrystalline dielectric materials such as investigated here are directly influenced by materials composition, structure and arrangement of phases. In the case of heterogenous materials such as ceramics, local variation in thermal parameters can occur because of the presence of different solid phases, pores, boundary

resistance, etc and thereby affect the propagation of thermal energy carriers [28-32]. The appearance of porosity amounts to a new phase in ceramic materials prepared through the gel route. In the case of porous ceramics, heat transport could be primarily due to two processes, phonon and radiative transport [33]. The former relates to the movement of atoms in the crystalline lattice, whereas the latter is due to electron transitions between energy levels in these atoms. If we neglect the relation between energy levels and spacing between the atoms, then both mechanisms can be considered independently. Such an assumption seems to be reasonable if the amplitude of atomic oscillations is considerably smaller than the lattice constant [22]. In general, the radiative contribution arises from photon emission caused by electron transport. However, in the case of dielectrics at room temperature, the density of electrons is negligibly small and thermal energy is carried mainly by phonons. The influence of pores on thermal conductivity value has already been investigated [31-33]. For cases in which the damping wavelength of thermal waves $L_{th} = 2\pi d$ is greater than or of the order of typical grain size (L), "thermal disturbance" is not affected by the heterogeneity of sample and the measurements then yield the "global thermal diffusivity" [34], which is the case for all samples in the present study. However, the pores in the lattice can act as scattering centres for phonons and hence affect the phonon mean free path and consequently their thermal diffusivity value. **Results of pore size distribution and N_2 adsorption characteristics of cerium phosphate gel after calcination at 400 ^{0}C and 800 ^{0}C are given in Figures 6 (a) and 6 (b) respectively. The presence of micropores (<20 Å) with extended mesoporosity (20-500 Å) is seen in calcined gels.** On heating to 800 °C volume of smaller pores up to around 100 Å decreases considerably and correspondingly decrease in surface area from 96 to 49 m^2/g is observed when the gel is heated at 400 ^{0}C and 800 ^{0}C respectively. The BET isotherms with characteristic loop clearly indicate a type IV, i.e., mainly mesoporous textures, although at relatively low pressure (P/P0) it shows microporous character. Compared with 800 ^{o}C calcined sample, the volume of adsorption of N_2 is much higher in the case of 400 ^{o}C

calcined sample at all relative pressure. Generally, as the pore sizes are much smaller than the damping wavelength of thermal waves, the measured values in this study are the effective thermal parameters of specimen.

As reported earlier [28-30], density variations and hence porosity variations caused by sintering temperature of samples under investigation can affect the thermal conductivity value. By considering porous ceramics as a two-phase network in which pores are randomly embedded in a solid matrix, the thermal diffusivity of the specimen is given by the expression, $k_c(p) = \frac{K_c(p)}{\rho_0 C_0 (1-p)}$, where $K_c(p)$ is the thermal conductivity of the specimen having porosity p. ρ_0 and C_0 are the density and specific heat capacity of the sample with zero porosity [35]. If the thermal conductivity of the porous material is modified by the same ratio as that of the ratio between actual density and maximum density, then thermal conductivity is given by Leob equation [36], $K_c(p) = K_0(1-p)$. However, such a methodology to evaluate thermal conductivity yields thermal diffusivity value that is independent of porosity, which contradicts our experimental observation. All the studies done on samples prepared via sol-gel route show a dependence of thermal diffusivity value on porosity. A similar influence of porosity on heat transport of ceramics has already been investigated [37]. In order to incorporate the influence of porosity on the propagation of thermal waves and hence on the measured thermal diffusivity values, Sanchez-Lavega et.al [38] modified the Leob equation for thermal diffusivity as $k_c(p) = k_0 \frac{(1-np)}{(1-p)}$, where n is an empirical constant. From table I, it is clear that the measured thermal diffusivity values agree well with that calculated using modified Leob equation. Increase in density and a consequent decrease in porosity with sintering temperature results in a proportional reduction in scattering centers for phonons with sintering temperature, which consequently affects the phonon mean free path. The lattice thermal conductivity (thermal diffusivity) which is also proportional to phonon mean free path, thus varies in accordance with variations in porosity. Dependence of thermal diffusivity of all the

samples under investigation on porosity indicates that the samples are below their percolation threshold. Percolation threshold is the limit above which a specific physical property (e.g, thermal diffusivity, hardness, stiffness etc) is insensitive to further changes in relative density. Above percolation threshold, particle-particle contact is insufficient to fully transmit the physical forces [23].

The calculated value of empirical constant n (=1.98) > 1 suggests that the effect of porosity on heat conduction in all the samples under study is not a mere density effect (air holes in the bulk specimen). A value of $n = 1$ suggests that thermal diffusivity value becomes equal to k_0 and thus thermal diffusivity value is independent of porosity. A value of $n < 1$ suggests that porous ceramics can exhibit higher thermal diffusivity value compared to samples with zero porosity, which contradicts our experimental observation as well as the scattering mechanisms in porous ceramics. Evaluation of thermal conductivity using the relation thus affects the propagation of phonons through the specimen, apart from porosity (or density). In the case of larger grain sized nanocrystals, majority of heat is carried away by well defined quanta of propagating and polarized vibrational modes (i.e phonons). Hence the actual value of thermal parameters is determined by the mean free path of phonons between the scattering events. Mean free path of phonons are essentially determined by various scattering mechanisms in ceramics such as phonon-phonon scattering, phonon-electron scattering, phonon-grain boundary scattering, phonon-defect scattering, etc [30]. In the case of samples investigated here, phonon-electron scattering can be neglected as the densities of free electrons are negligibly small. However, grain boundaries affect the propagation of phonons and hence their thermal diffusivity value. If the grain boundary has a significant thickness, phonons will be scattered a few times inside the grain boundary phase and the thermal conductivity of grain boundary phase plays a significant role in determining the effective thermal parameters. If the grain boundaries are thin enough, phonons may scatter once at the grain boundary and then the phonon scattering sites in sample grains will control the effective

thermal parameters of sintered samples [39]. SEM analysis of our samples sintered at 1300^0C (Figure 7) and 1500^0C (Figure 8) shows that grain size increases from 1 µm to 2 µm for samples sintered at 1300^0C and 1500^0C respectively. As the sintering temperature increases, grain size increases resulting in reduction in grain boundaries and a consequent increase in phonon mean free path and hence thermal diffusivity value. A recent investigation shows that for dense samples, the phonon mean free path is smaller than the grain size at all processing temperatures [40]. Hence, in addition to porosity, the defects in grains also contribute to the variation in thermal diffusivity [41] and this explains the value of n >1. An investigation on porous ceramic alumina shows that the solid area fraction (SAF) in the direction of heat flow also affects the measured thermal diffusivity value [23]. Enhancement in solid area fraction with increase in sintering temperature results in cohesive thermal transport with reduced scattering due to defects and interfaces. Thermal contact resistance (R_T) at the interface is related to macroscopic thermal conductivity (K_c) and to the grain conductivity (K) through the relation $\frac{L}{K_c} = \frac{L}{K} + R_T$, where L is the grain size [42]. Increase in sintering temperature results in enhanced contribution from grain conductivity due to more ordered structure and reduction in interface thermal resistance.

Conclusions:

In this article, we measured the thermal diffusivity value of $CePO_4$ prepared by the sol-gel process using laser induced nondestructive photoacoustic technique. Present study clearly shows that sintering temperature and consequent variation in porosity alters the scattering centre concentration for phonons propagating through the lattice. From the analysis of results, it is evident that the transient thermophysical parameter, viz., thermal diffusivity, varies substantially with sintering temperature. An empirical relation of thermal diffusivity on porosity shows that propagation of phonons and hence thermal diffusivity value is not merely affected by porosity, but by other factors such as grain boundary resistance and interface

thermal resistance. The present investigation also shows that, by measuring thermophysical parameters, the simple and elegant PA technique can throw light into structural variations of ceramics caused by variations in processing conditions. Such tunability in thermal properties with processing conditions and evaluation of thermal diffusivity of these materials could find applications in the microelectronic and optolectronic industry.

References

1) J.Sun, Int. J. Cerm. Technol, 4(1), (2007), p.75.
2) Q. Huang, L.Gao, Y. Liu, J. Sun, J. Mater. Chem.,15 (20), (2005), p.1995.
3) K. Popa, D. Sedmidubsky, O. Benes, C. Thiriet, R. J. M. Konings, J. Chem.Thermodynamics,, 38, (2006), p.825.
4) H. Meyssamy, K. Riwotzaki, A. Kronowski, S. Naused, M.Hasse, Adv. Mater. 11(10), (1999), p.840.
5) P.E.D. Morgan, D. B. Marshall, J. Am. Ceram.Soci., 78 (6), (1995), p.1553.
6) Y. Hikichi and T. Nomura, J. Am. Cerm. Soci., 70(10), (1987), C-252.
7) L. A. Boatner, M. M. Abraham, B. C. Sales, Inorg. Chim. Acta, 94, (1984), p.146.
8) T. Norby, N. Christiansen, Solid. Stat. Ionics, 77, (1995), p.240.
9) Y. Hikichi and T. Ota, Phosphorus Res. Bull. 6, (1996), p.175.
10) Y. Hikichi and T. Ota, Miner. J. 19(3), (1997), p.123.
11) S. Lucas, E. Champion, D. Bernache-Assollant, G. Leroy, J. Sol. State.Chem., 177, (2004), p.1312.
12) L. Karpowicha, S. Wilckeb, Rong Yuc, G. Harleya, J.A. Reimerb, L.C. De Jonghe, J. Sol. State.Chem., 180, (2007), p.840.
13) D. Bregiroux, S. Lucas, E. Champion, F. Audubert, D. Bernache-Assollant, J. Euro. Ceramic Society, 26, (2006), p.279.
14) A. Rosencwaig and A. Gersho, J. Appl. Phys. 47, (1976), p.64.
15) A. Mandelis, S. B. Peralta and J. Thoen, Journal of Applied Physics, 70(3), (1991),p.1761.
16) M. Chirtoc, I.Chirtoc,S. Pittois, C. Glorieux and J. Thoen, Review of Scientific Instruments, 74 (1 II), (2003), p.632.
17) B. Li and E. Welsch, Applied Optics, 38 (24), (1999), p.5241.

18) S. D. George, P. Radhakrishnan, V. P. N. Nampoori, and C. P. G. Vallabhan, Phys. Rev. B, 68, (2003), p.163519.

19) S. D. George, S. Saravanan, M. R. Anantharaman, S. Venketachalam, P. Radhakrishnan,V. P. N. Nampoori and C. P.G. Vallabhan, Phys. Rev. B, 69, (2004), p.235201.

20) S. D: George, P. Radhakrishnan, V. P. N. Nampoori, and C. P. G. Vallabhan, J. Phys. D: Appl. Phys., 36, (2003), p.990.

21) S. D. George, R. Komban, K. G. K. Warrier, P. Radhakrishnan, V. P. N. Nampoori and C.P.G. Vallabhan, International Journal of Thermophysics, 28(1), (2007), p.123.

22) L. Braginsky, V. Shklover, H. Hofmann, P. Bowen, Phy. Rev. B, 70, (2004), p.134201.

23) E. J. Gonzalez, G.White, L. Wei, J. Mater. Res. 15(3), (2000), p.744.

24) W. M. Lima, V. Biondo, W. R. Weinand, E. S. Nogueira, A. N. Medina, M. L. Baesso and A. C. Bento, J. Phys.Condens.Matter, 17, (2005), p.1239.

25) D. Jia, D. K. Kim, W. M. Kriven, J. Am. Ceram. Soc. 90(6), (2007), p.1760.

26) S. D. George, Aji A Anappara, K. G. K. Warrier, P. Radhakrishnan, V. P. N. Nampoori and C. P. G. Vallabhan, Mater. Chem. Phys. 111 (2008) p.38 .

27) S. D. George, Saji Augustine, Elizabeth Mathai, P. Radhakrishnan, V. P. N. Nampoori and C. P. G. Vallabhan, Phys. Stat. Solidi (a), 196(2), (2003), p.384.

28) S. Fayette, D. S. Smith, A. Smith, C. Martin, J. Euro. Cerm. Society, 20, (2000), p. 297.

29) H. Szelagowski, I. Arvanitidis, S. Seetharaman, J. Appl. Phys. 85(1), (1999), p.193.

30) K. Watari, K. Ishizaki, F. Tsuchiya, J. Mater. Sci., 28, (1993), p.3709.

31) B. Nait-Ali, K. Haberko, H. Vesteghem, J. Absi, D. S. Smith, J. Euro. Cerm. Society, 26, (2006), p.3657.

32) Z.Y. Deng, J. M. F. Ferreira, Y. Tanaka, Y. Isoda, Acta. Mater.,55, (2007), p.3663.

33) L. Berginsky,V. Shklover, G. Witz and H. P. Bossmann, Phys.Rev. B, (2007), p.94301.

34) E. Litoysky, T. Gambaryan-Roisman, M. Shapiro, and A. Shavit, Trends in Heat, Mass and Momentum Transfer, Vol. 3 (Council of Scientific Research Integration, Trivandrum, India), (1997), 147.

35) J. F. Kerrisk, J. Appl. Phy. 42, (1971), p.267.

36) H. W. Codbee, W. T: Ziegler, J. Appl. Phys. 37, (1966), p.56.

37) D. M. Liu, Ch. J. Chen, and L. J. Lin, J. Appl. Phys. 75, (1994), p.3765.

38) A. Sanchez-Lavega, A. Salazar, A. Ocariz, L. Pottier, E. Gomez, L. M. Villar, and E.Macho, Appl. Phys. A 65, (1997), p.15 and references therein.

39) Z. Zhong, W. Wang, J. Appl. Phys, 100, (2006), p.44310.

40) R. W. Rice, J. Mater. Sci. 31, (1996), p.102.

41) K. Watari, H. Nakano, K. Sato, K. Urabe, K. Ishisaki, S. Cao, and K. Mori, J. Am. Ceram. Soc. 86, (2003), p.1812.

42) M. V. Swain, L. F. Johnson, R. Syed, and D. P. H. Haseelman J. Mater. Sci. Lett. 5, (1998), p.799.

Table 1. Thermal diffusivity of $CePO_4$ ceramics

Figure Captions

Figure 1. **M** – monazite, **H** – hexagonal, **R**- rhabdophane,

X-ray diffraction pattern of cerium phosphate precursor gel heated at different temperature

(a) 400^{0}C (b) 800^{0}C (c) 1000^{0}C (d) 1300^{0}C (e) 1700 °C.

Figure 2. Plot of crystalline size versus temperature

Figure 3. Schematic view of experimental setup

Figure 4. Geometry of Photoacoustic configuration

Figure 5. Log-log plot of PA amplitude of $CePO_4$ sintered at 800^{0}C

Figure 6 (a). Pore size distribution of cerium phosphate precursor gel after calcinations at (a) 400 and (b) 800^{0}C

Figure 6 (b) N_2 adsorption isotherm of cerium phosphate precursor gel after calcinations at (a) 400 and (b) 800^{0}C

Figure 7. SEM of cerium phosphate sintered at 1300^{0}C

Figure 8. SEM of cerium phosphate sintered at 1500^{0}C

Table I

Sintering Temperature (^{0}C)	Porosity (%)	Measured thermal diffusivity value (cm^2s^{-1})	Calculated value of thermal diffusivity (cm^2s^{-1})
800	46	0.140 ± 0.004	0.142
900	42	0.250 ± 0.007	0.252
1000	38	0.342 ± 0.006	0.344
1100	27.5	0.534 ± 0.008	0.540
1200	4.3	0.820 ± 0.004	0.822
1300	0.5	0.846 ± 0.005	0.855
1400	1	0.846 ± 0.007	0.851
1500	2.5	0. 840 ± 0.004	0.847
1600	6.5	0. 790 ± 0.008	0.801
1700	8	0.786 ± 0.006	0.793

Figure 1.

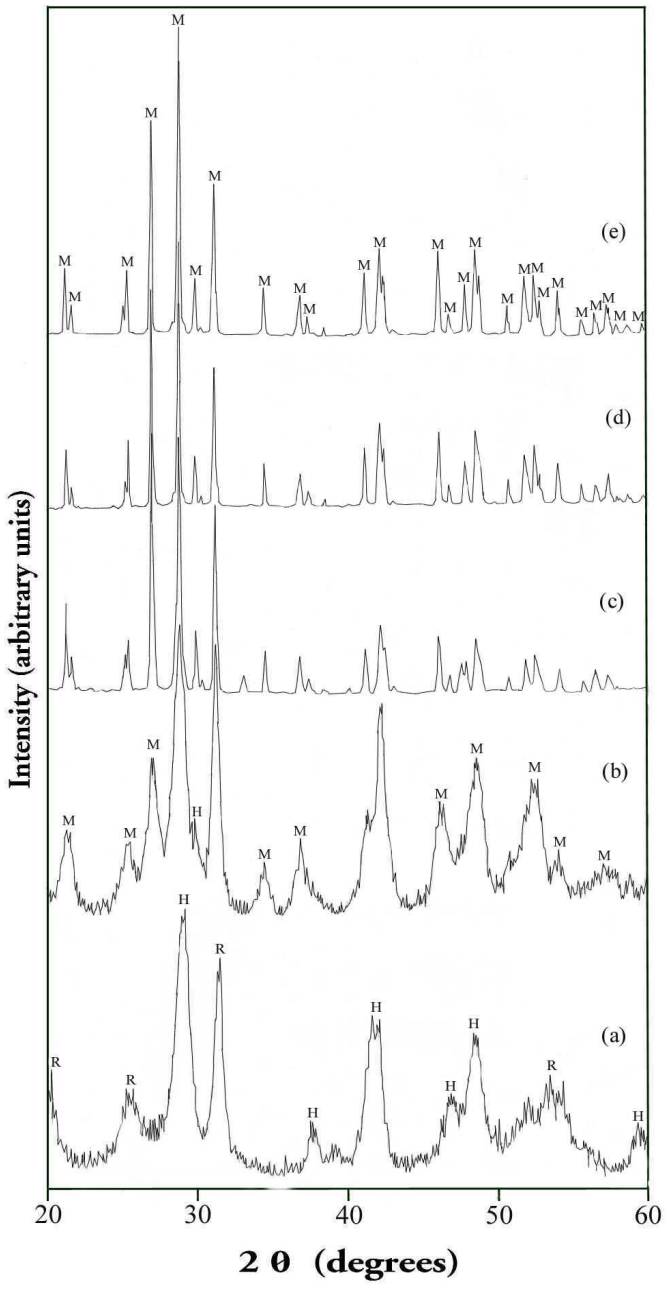
Intensity (arbitrary units)
2 θ (degrees)
20
30
40
50
60
(a)
(b)
(c)
(d)
(e)
M
H
R

Figure 2

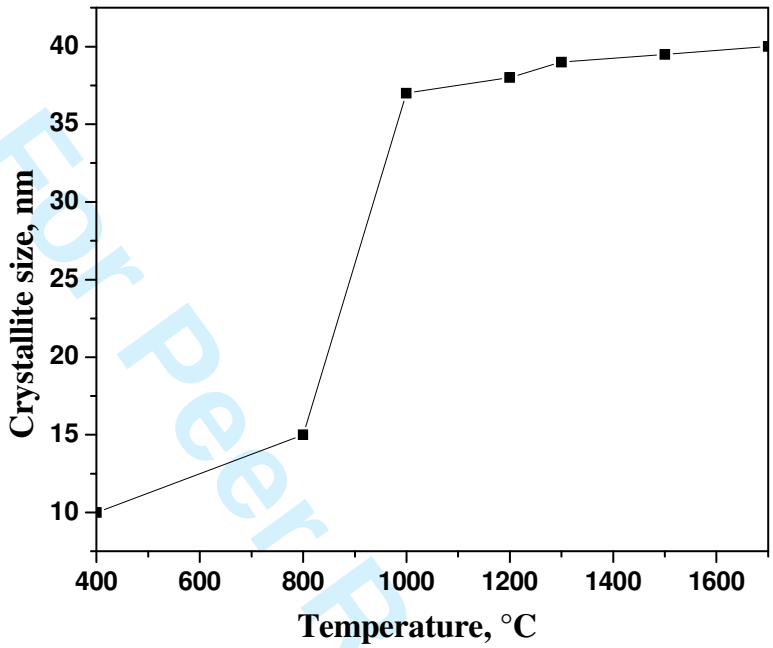

Figure 3

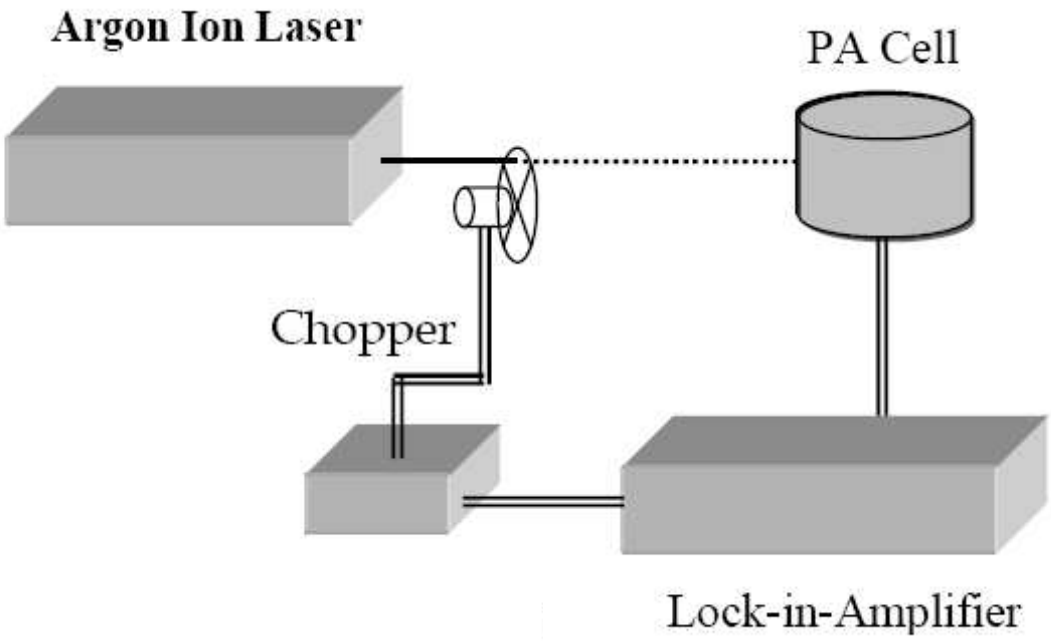

Figure 4

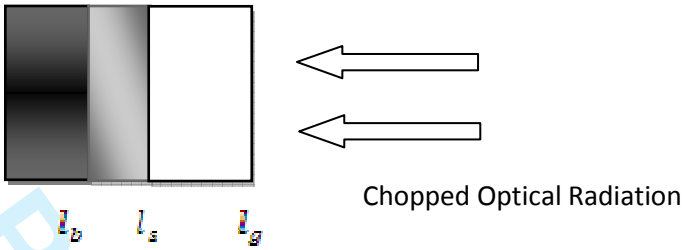

Figure 5

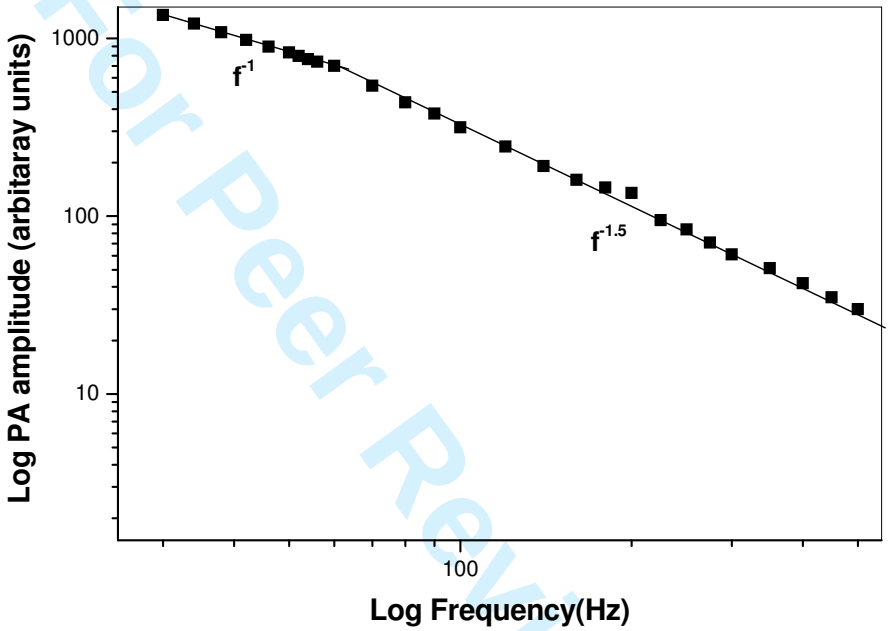

Figure 6 (a)

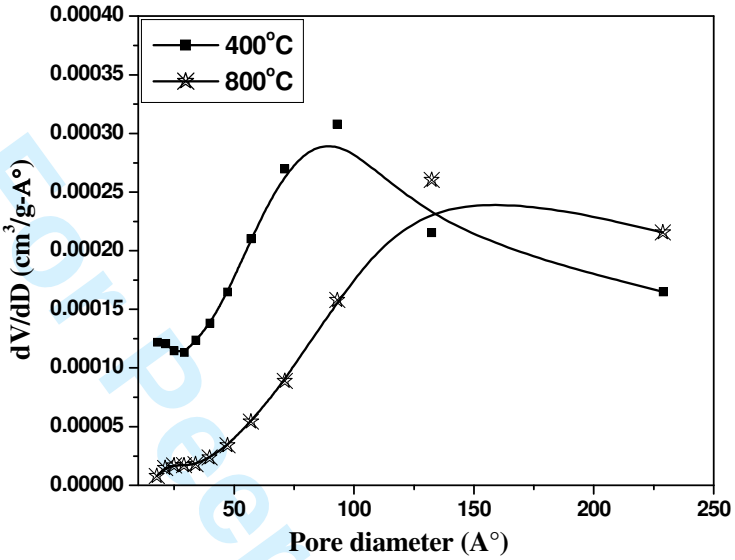

Figure 6 (b)

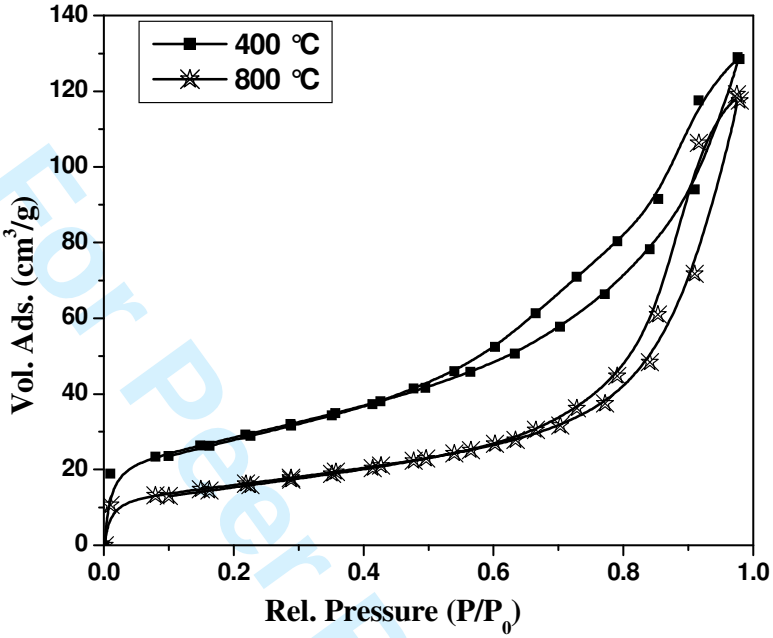

Figure 7

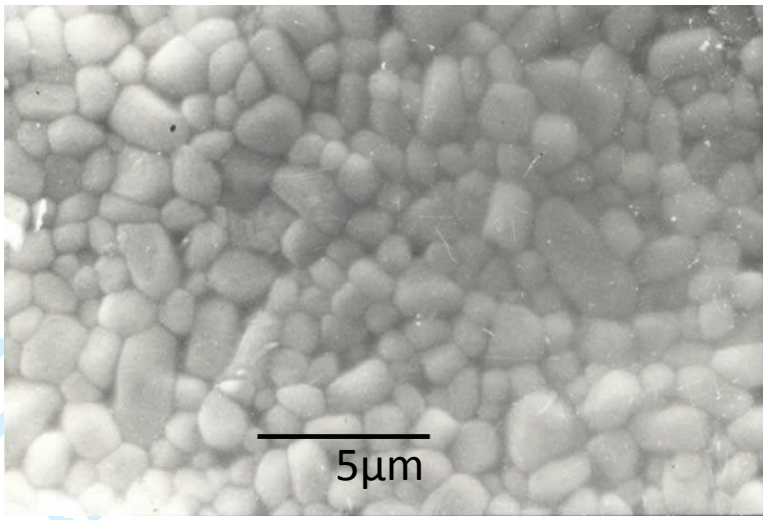

Figure 8